Statistical mechanics and computer simulation of systems with attractive positive power-law potentials

Lj. Milanović and H. A. Posch
Institut für Experimentalphysik, Universität Wien, Boltzmanngasse 5, A-1090 Wien, Austria

W. Thirring
Institut für Theoretische Physik, Universität Wien, Boltzmanngasse 5, A-1090 Wien, Austria

(Received 16 June 1997; revised manuscript received 14 October 1997)

We study many-body systems in d dimensions interacting with a purely attractive pair potential $\sim|\mathbf{x}_i-\mathbf{x}_j|^\nu$, where $\mathbf{x}_i$ is the position vector of particle i, and ν is a positive parameter. We derive the temperature in microcanonical equilibrium for arbitrary ν and d and, for $d=1$, the corresponding velocity distribution for a finite number N of particles. The latter reduces to the Maxwell-Boltzmann distribution in the infinite-particle limit. The one-dimensional particle distribution of the equilibrium cluster in the mean-field limit is computed numerically for various potential parameters ν. We test these theoretical expressions by comparing them to extensive computer simulation results of one-dimensional systems and find close agreement for $\nu=1$ (the sheet model) and $\nu=4.5$. In similar simulations for $\nu=1.5$ the macroscopic relaxation time exceeded the length of our simulation runs and the system did not relax towards the known microcanonical equilibrium state. We also compute full Lyapunov spectra for the linear sheet model and find that the Kolmogorov-Sinai entropy starts to increase linearly with N for $N>10$. [S1063-651X(98)01603-1]

PACS number(s): 05.45.+b, 02.70.Ns, 05.20.−y, 05.70.Ln

I. INTRODUCTION

We consider a system of N particles in d dimensions and with total energy E, described by the Hamiltonian

$$H=\sum_{i=1}^{N}\frac{\mathbf{p}_i^2}{2m_i}+\frac{\lambda}{N}\sum_{i=1}^{N-1}\sum_{j>i}^{N}\left|\frac{\mathbf{x}_i-\mathbf{x}_j}{\sigma}\right|^\nu, \tag{1}$$

where $\mathbf{x}_i\in\mathbf{R}^d$, $\mathbf{p}_i\in\mathbf{R}^d$, and m_i are the position, momentum, and mass of particle i, respectively, and $\nu\in\mathbf{R}^+$ is a positive parameter. The total energy is E. The pair potential is of infinite range and purely attractive, $\lambda\in\mathbf{R}^+$, $\sigma\in\mathbf{R}^+$, and the particles may pass freely through each other. Starting from any initial condition such a system is expected to relax towards a state of thermodynamic equilibrium characterized by a symmetrical cluster distribution of the particles in d-dimensional space, and—for $N\to\infty$—by the Maxwell-Boltzmann distribution in momentum space.

The scaling factor $1/N$ for the potential energy in Eq. (1) is required for the large-particle limit $\{N\to\infty, H/N=\epsilon,\ \epsilon$ finite$\}$ to exist. This limit is equivalent to the Vlasov (or continuous-system) limit $\{N\to\infty, \mathcal{H}\equiv H/N=\epsilon, s\equiv m/N\to 0,\ \epsilon$ and m finite$\}$ [1] of the rescaled Hamiltonian $\mathcal{H}$,

$$\mathcal{H}\equiv\frac{H}{N}=\sum_{i=1}^{N}\frac{\tilde{\mathbf{p}}_i^2}{2s}+\frac{\lambda}{N^2}\sum_{i=1}^{N-1}\sum_{j>i}^{N}\left|\frac{\mathbf{x}_i-\mathbf{x}_j}{\sigma}\right|^\nu, \tag{2}$$

where $\tilde{\mathbf{p}}_i=\mathbf{p}_i/N$ are the scaled momenta. In this representation the total mass $m\equiv Ns$ and the total energy $\epsilon\equiv E/N$ are *finite*. For simplicity we have assumed here that the scaled particle mass, $s=m/N$, is the same for all particles.

For the special case $d=1$ and $\nu=1$ the scaled Hamiltonian (2) applies to a system of N infinite parallel mass sheets, where each sheet extends over a plane parallel to the yz plane and moves along the x axis under the mutual gravitational attraction of all the other sheets [2,3]. If the uniform mass density of a sheet is identified with $s\equiv m/N$, the Hamiltonian of the sheet model is usually written in the form

$$\mathcal{H}=\sum_{i=1}^{N}\frac{\tilde{p}_i^2}{2s}+2\pi G s^2\sum_{i=1}^{N-1}\sum_{j>i}^{N}|x_i-x_j|, \tag{3}$$

where G is the universal gravitational constant. As is common practice we will refer to the sheets also as particles of mass s, moving along the x axis. The mutual crossing of two such particles will also be referred to as a collision. The total mass of the system, Ns, is equal to the mass m of a single particle for the unscaled model (1), and the total energy is finite, $\mathcal{H}=\epsilon$.

The linear sheet model was originally proposed as a model for the dynamics of stars transverse to the galactic plane of a highly flattened galaxy [2,3], and was recognized to be of relevance also for plasma physics [4]. Most important, however, it has been widely used as a simple model for studying the surprisingly weak and unclear ergodic properties and complicated relaxation behavior of gravitational systems [5–9]. It was originally suggested by Hohl [10,11] that nonequilibrium states relax to (microcanonical) equilibrium on time scales of order N^2t_c, where t_c is a typical oscillation period of a particle. Subsequent studies by Wright and Miller [12,13] established, however, that the actual relaxation time is typically orders of magnitude larger than this prediction and depends strongly on the initial conditions. Furthermore, systems with only a few sheets, $N\leqslant 10$, have been shown to be not even ergodic [14,7]: regularity islands with a finite measure in phase space exist and prevent the existence of a microcanonical equilibrium state in this case. For larger systems the relaxation towards equilibrium proceeds through a

number of intermediate and long-lived quasistationary states [15,16,9]. In spite of all this work it is still not clear whether the one-dimensional sheet model relaxes for $N>10$ towards a microcanonical equilibrium starting from an arbitrary initial condition. There is numerical evidence, however, that microcanonical equilibrium may be reached for a two-component mixture of mass sheets with a mass ratio of 1:3 [17].

A condition for the existence of microcanonical equilibrium is that the phase trajectory is fully Lyapunov unstable: All the Lyapunov exponents must be different from zero, with the exception of those directly associated with the macroscopically conserved quantities and the nonexponential expansion in the direction of the phase flow. In the case of the linear sheet model this amounts to four vanishing exponents. If the energy hypersurface is ergodic, the existence of a single positive exponent usually implies that altogether $N-2$ positive exponents exist. If one considers a whole set of different initial conditions in a small box on the energy surface, the time constant for spreading these points over the energy surface by the flow is given by $1/h_{\rm KS}$, where $h_{\rm KS}$ is the Kolmogorov-Sinai entropy [19,18]. For ergodic Hamiltonian systems $h_{\rm KS}$ is equal to the sum of all positive Lyapunov exponents [20]. The Kolmogorov-Sinai entropy was computed for the sheet model by Benettin, Froeschle, and Scheidecker [21] for $N\leqslant 10$ and was conjectured to increase linearly with N. Since this range corresponds to nonergodic systems with an energy surface decomposed into a regular region embedded in a chaotic sea [14], we have extended these computations to larger systems containing 16 or 24 sheets and which are believed to be ergodic and mixing [7].

This paper is organized as follows. Section II is concerned with the microcanonical equilibrium properties. In Sec. II A we consider the most general case of a d-dimensional system (1) with arbitrary positive potential parameter ν, and derive, within the framework of the microcanonical ensemble, the exact relation between temperature and energy for a finite number N of particles. For $d=1$ and $\nu=1$ our results reduce, up to order $O(1/N)$, to the well-known expressions for the sheet model first obtained by Rybicki [22]. For the remainder of the paper we shall restrict ourselves only to the linear case, $d=1$. In Sec. II B the momentum distribution $\rho_N(p)$ for linear N-particle systems with arbitrary $\nu>0$ is derived. For $\nu=1$ this expression is identical to the familiar result for the sheet model [22]. In Sec. II C we discuss the particle density distribution $n(x)$ in the mean-field limit, where we make use of the canonical ensemble. And in Sec. III we outline Benettin's exact algorithm [21] for the numerical computation of the full spectrum of Lyapunov exponents for the sheet model.

In Sec. IV we compare our theoretical results to extensive computer simulations for one-dimensional systems and for selected values of the potential parameter ν. For $\nu=1$, the sheet model, full Lyapunov spectra for systems containing 10, 16, and 24 particles are presented in Sec. IV A. For larger systems only the two largest exponents were computed. In Sec. IV B we study the relaxation properties of systems with $\nu=1.5$ and find, surprisingly, an even stronger tendency to remain in very stable quasistationary nonequilibrium states than for $\nu=1$. Systems with $\nu=4.5$, however, display ''normal'' relaxation and mixing behavior, as shown in Sec. IV C. We conclude in Sec. V with a discussion of our results and a few remarks concerning the relaxation of these systems towards equilibrium.

II. MICROCANONICAL EQUILIBRIUM PROPERTIES

A. The microcanonical temperature for arbitrary d and $\nu>0$

Let ω denote a state point in the full $2dN$-dimensional phase space, and $d^{2dN}\omega\equiv\Pi_{i=1}^{N}d^dx_i d^dp_i$. Then the microcanonical entropy $S(E)$ is given by

$$e^{S(E)/k}=C\int d^{2dN}\omega\,\delta(E-H)\,\delta^d\Bigg(\mathbf{X}-\sum_i \mu_i\mathbf{x}_i\Bigg)\times\delta^d\Bigg(\mathbf{P}-\sum_i \mathbf{p}_i\Bigg)\delta^{d(d-1)/2}\Bigg(\mathbf{L}-\sum_i \mathbf{l}_i\Bigg),\qquad(4)$$

where the Hamiltonian H is given by Eq. (1). E is the total energy of the system, k is Boltzmann's constant, and $\mu_i\equiv m_i/\Sigma_{j=1}^{N}m_j$ is the relative mass of particle i. C is a normalization constant. The δ functions constrain the contributing states to the hypersurface characterized by the constants of motion: (i) energy, $H=E$; (ii) center of mass, $\mathbf{X}=\Sigma_{i=1}^{N}\mu_i\mathbf{x}_i$; (iii) total linear momentum, $\mathbf{P}=\Sigma_{i=1}^{N}\mathbf{p}_i$. The condition of stationarity requires $\mathbf{P}=0$; (iv) total angular momentum, $\mathbf{L}=\Sigma_{i=1}^{N}\mathbf{l}_i$, where $\mathbf{l}_i=\mathbf{x}_i\times\mathbf{p}_i$ is the angular momentum of particle i. $\mathbf{L}$ is a pseudovector with $d(d-1)/2$ independent components.

The constrained hypersurface has $2dN-[1+2d+d(d-1)/2]$ dimensions, which reduces to $2N-3$ dimensions for the linear problem, $d=1$. In addition to $\mathbf{P}=\mathbf{0}$ we take for the following also $\mathbf{X}=\mathbf{0}$, which can always be achieved with a simple translation. Furthermore, we restrict ourselves to the special case of vanishing angular momentum, $\mathbf{L}=\mathbf{0}$. With this simplification, and rewriting the condition for energy conservation, we obtain

$$e^{S(E)/k}=\frac{C}{E}\int d^{2dN}\omega\,\delta\Bigg(1-\frac{H}{E}\Bigg)\delta^d\Bigg(\sum_i \mu_i\mathbf{x}_i\Bigg)\delta^d\Bigg(\sum_i \mathbf{p}_i\Bigg)\delta^{d(d-1)/2}\Bigg(\sum_i \mathbf{l}_i\Bigg).\qquad(5)$$

With the transformation $\mathbf{p}\to\sqrt{E}\mathbf{p}'$ and $\mathbf{x}\to(E/\lambda)^{1/\nu}\mathbf{x}'$ the whole E dependence may be factored out from this integral, and one obtains

$$e^{S(E)/k}=CE^{d(1/2+1/\nu)(N-d/2-1/2)-1}\int d^{2dN}\omega'\,g(N,\nu,d,\lambda)\,\delta(1-H')\,\delta^d\Bigg(\sum_i \mu_i\mathbf{x}'_i\Bigg)\delta^d\Bigg(\sum_i \mathbf{p}'_i\Bigg)\delta^{d(d-1)/2}\Bigg(\sum_i \mathbf{l}'_i\Bigg)$$
$$=E^{d(1/2+1/\nu)(N-d/2-1/2)-1}I(N,\nu,d,\lambda),\qquad(6)$$

where the primed quantities refer to the new coordinates $\mathbf{x}_i'$ and momenta $\mathbf{p}_i'$, and the transformed Hamiltonian is given by

$$H' \equiv \frac{H}{E} = \sum_{i=1}^{N} \frac{\mathbf{p}'^2_i}{2m_i} + \frac{1}{N} \sum_{i=1}^{N} \sum_{j>i} \left| \frac{\mathbf{x}'_i - \mathbf{x}'_j}{\sigma} \right|^{\nu}.$$

The function $g(N,\nu,d,\lambda)$ and the related integral $I(N,\nu,d,\lambda)$ do not depend on the energy E and will not concern us further. We finally obtain for the entropy

$$S(E)/k = \left\{ \left(\frac{d}{2} + \frac{d}{\nu} \right) \left(N - \frac{d}{2} - \frac{1}{2} \right) - 1 \right\} \ln E + \ln I(N,\nu,d,\lambda)$$

for $d \geqslant 1$. The microcanonical temperature follows from

$$\frac{1}{T} = \frac{\partial S}{\partial E}$$

and yields

$$kT = \frac{E}{(d/2 + d/\nu)(N - d/2 - 1/2) - 1}. \tag{7}$$

It reduces to

$$kT = \frac{E}{(N-1)(1/2 + 1/\nu) - 1} \tag{8}$$

for the linear case, $d=1$, for which angular momentum conservation does not contribute. The last equation can be compared for $\nu = 1$ to an expression of Rybicki [22], which differs from Eq. (8) by a term of order $O(1/N)$. However, the temperature-energy relation in [22] was obtained with the canonical ensemble, which is known to give results that may differ from the microcanonical ones by terms of precisely that order.

The partition into kinetic and potential energy is a well-known consequence of the virial theorem,

$$\overline{K} = \frac{\nu}{2} \overline{V}, \tag{9}$$

where the bar denotes a time average.

B. Momentum distribution for one-dimensional systems

The derivation of the momentum distribution is slightly more involved than that of the temperature, but proceeds with similar arguments as before. For one-dimensional systems angular momentum conservation does not apply and the last δ function in Eq. (4) is missing. Performing the integration in Eq. (4) over the full configuration space and over the momentum subspace of particles 2 to N, $d^{(2N-1)}\omega \equiv \Pi_{i=1}^{N} dx_i \Pi_{i=2}^{N} dp_i$, we obtain for the momentum distribution of an arbitrary particle 1,

$$\rho_N(p_1) = C_1 e^{-S(E)/k} \int d^{(2N-1)}\omega \, \delta(E - H) \, \delta^d \left(\sum_i \mu_i x_i \right) \delta \left(\sum_i p_i \right), \tag{10}$$

where C_1 is a normalization constant. We assume that the mass of all particles is equal, $m_i = m$, and consequently $\mu_i = \mu$ for all i. With the transformation $p_i \to p_i' - p_1/(N-1)$ $(\forall i > 1)$, and $d^{(2N-1)}\omega' \equiv \Pi_{i=1}^{N} dx_i \Pi_{i=2}^{N} dp_i'$, we obtain

$$\rho_N(p_1) = C_1 e^{-S(E)/k} \int d^{(2N-1)}\omega' \, \delta \left(E - \frac{p_1^2}{2m} - \sum_{i=2}^{N} \frac{[p_i' - p_1/(N-1)]^2}{2m} - \frac{\lambda}{N} \sum_{i=1}^{N-1} \sum_{j>i}^{N} \left| \frac{x_i - x_j}{\sigma} \right|^{\nu} \right)$$
$$\times \delta \left(\sum_i \mu x_i \right) \delta \left(p_1 + \sum_{i=2}^{N} \left(p_i' - \frac{p_1}{N-1} \right) \right),$$

which, with $\Sigma_{i=2}^{N} p_i' = 0$ and the notation

$$H' \equiv \sum_{i=2}^{N} \frac{p'^2_i}{2m} + \frac{\lambda}{N} \sum_{i=1}^{N-1} \sum_{j>i}^{N} \left| \frac{x_i - x_j}{\sigma} \right|^{\nu},$$

$$E' \equiv E - \frac{N}{N-1}\frac{p_1^2}{2m}$$

leads to

$$\rho_N(p_1) = C_1 e^{-S(E)/k} \int d^{(2N-1)}\omega'\, \delta(E'-H')\, \delta\left(\sum_{i=1}^{N} \mu x_i\right) \delta\left(\sum_{i=2}^{N} p_i'\right).$$

As before, center-of-mass coordinates are used, for which $X=0$ and $P=0$. With the transformation $p' \to \sqrt{E'}p''$, $x \to (E'/\lambda)^{1/\nu}x''$ the whole E' dependence may be factored out of the integral,

$$\rho_N(p_1) = E'^{(N-1)(1/\nu+1/2)-3/2} e^{-S(E)/k} J(N,\nu,\lambda) = E^{(N-1)(1/\nu+1/2)-3/2}\left(1-\frac{N}{N-1}\frac{p_1^2}{2mE}\right)^{(N-1)(1/\nu+1/2)-3/2} e^{-S(E)/k} J(N,\nu,\lambda),$$

where the remaining integral $J(N,\nu,\lambda)$ depends only on the indicated parameters. Insertion of Eq. (6) for $d=1$ yields

$$\rho_N(p_1) = \frac{1}{\sqrt{E}}\left(1-\frac{N}{N-1}\frac{p_1^2}{2mE}\right)^{(N-1)(1/\nu+1/2)-3/2} \frac{J(N,\nu,\lambda)}{I(N,\nu,\lambda)}.$$

J/I is determined from

$$\int_{-p_{\max}}^{p_{\max}} dp_1 \rho_N(p_1) = 1,$$

where $p_{\max}$ is the largest momentum accessible to a single particle. For a system with energy E, for which the total momentum vanishes, the maximum energy transferable to a single particle is given by $(N-1)E/N$. Consequently, $p_{\max} = \sqrt{2mE(N-1)/N}$. With this, we finally obtain for the momentum distribution of a single particle:

$$\rho_N(p_1) = \frac{\Gamma((N-1)(1/\nu+1/2))}{\Gamma((N-1)(1/\nu+1/2)-1/2)}\sqrt{\frac{N}{2\pi(N-1)mE}}\left(1-\frac{N}{N-1}\frac{p_1^2}{2mE}\right)^{(N-1)(1/\nu+1/2)-3/2}. \tag{11}$$

This result generalizes an expression, first derived by Rybicki [22] for the sheet model with $\nu=1$, to general $\nu>0$.

If we replace the energy E in Eq. (11) by the temperature according to Eq. (7), we may perform the limit to large particle numbers at constant T. Since $\lim_{N\to\infty}(1-a/N)^N = e^{-a}$, we obtain

$$\lim_{N\to+\infty}\left(1-\frac{N}{N-1}\frac{p_1^2}{2mkT[(N-1)(1/\nu+1/2)-3/2-1/\nu]}\right)^{(N-1)(1/\nu+1/2)-3/2} = e^{-p_1^2/(2mkT)},$$

which, after normalization, becomes the familiar Maxwell-Boltzmann distribution in the thermodynamic limit:

$$\rho(p_1) = \sqrt{\frac{1}{2\pi mkT}} e^{-p_1^2/(2mkT)}. \tag{12}$$

C. Particle density for one-dimensional systems

In the limit of large N the force between individual particles becomes negligible as compared to the mean force exerted by all the other particles. Since the potential of mean force is given by the Poisson equation, and the dynamics of the one-particle distribution function is described by the collisionless Boltzmann (or Vlasov [23]) equation, the equilibrium distribution is a simultaneous and self-consistent stationary solution of these equations. For charged particles this idea may be traced back to Debye and Hückel [24,25], and was subsequently also applied to gravitating systems [3,26]. The computation of the equilibrium particle distribution $n(x)$ in this mean-field (or Vlasov) limit [1] is carried out within the framework of the canonical ensemble by maximizing the entropy functional with respect to $n(x)$ and passing to the limit $N\to\infty$. If x is measured relative to the center of mass, $n(x)$ becomes the solution of the self-consistency equation [27]

$$n(x) = n_0 \exp\left[-\beta \int dy \lambda \left|\frac{x-y}{\sigma}\right|^{\nu} n(y)\right]. \tag{13}$$

Here, $\beta \equiv 1/kT$ and n_0 are Lagrange multipliers, where n_0 ensures the proper normalization $\int dx n(x) = 1$. For an arbitrary $\nu \neq 1$ we solve this equation numerically by iterating a trial function for $n(x)$.

For the sheet model, $\nu=1$, the analytic solution of Eq. (13) is well known [3,22],

$$n(x) = \frac{\beta\lambda}{4\sigma}\cosh^{-2}\left(\frac{\beta\lambda x}{2\sigma}\right). \tag{14}$$

This may be verified by splitting the integral in the exponent of Eq. (13) according to $\int_{-\infty}^{+\infty}|x-y|n(y)dy=\int_{-\infty}^{x}(x-y)n(y)dy+\int_{x}^{+\infty}(y-x)n(y)dy$, and by noting that $\int dy y\cosh^{-2}y=y\tanh y-\ln\cosh y\rightarrow_{y\rightarrow\pm\infty}0$.

For the sheet model also the exact microcanonical particle distribution $n_N(x)$ for a finite particle number N is known. To facilitate the comparison with our computer-simulation data in Sec. IV A, we reproduce here also this well-known result of Rybicki [22]:

$$n_N(x)=\frac{\lambda(3N-5)}{2E\sigma}\sum_{j=1}^{N-1}A_j^N\left(1-\frac{j\lambda|x|}{E\sigma}\right)^{(3N-7)/2}, \quad (15)$$

where

$$A_j^N=\frac{[(N-1)!]^2(-1)^{j-1}j}{(N-1-j)!(N-1+j)!}.$$

$n_N(x)$ also approaches the canonical solution (14) in the mean-field limit [22].

III. LYAPUNOV SPECTRUM FOR THE SHEET MODEL

In this section we outline the method of Benettin [21] for the computation of all Lyapunov exponents for the linear sheet model, $\nu=1$. It was used recently by Tsuchiya *et al.* [15] to determine the largest exponent for systems containing up to 512 sheets. Here we apply it to the computation of the full Lyapunov spectrum for systems with $10\leqslant N\leqslant 24$. For $N>24$ only the two largest exponents are determined. The method requires the determination of the exact tangent-space dynamics [28–30] both for the constant-force streaming between collisions and for the interparticle crossing events. In the past also approximate methods were used for the maximum exponent [7,15], which were based on finite differences between neighboring trajectories in phase space. For ergodic systems the exact and approximate algorithms give comparable results [15].

Our restriction to the case $\nu=1$ is dictated by computer economy. The case $\nu\neq 1$ is computationally much more expensive and will be reported separately [31].

If $\mathbf{\Gamma}(t)=\{x_1,\ldots,x_N,p_1,\ldots,p_N\}$ denotes a state point in phase space, the phase flow is the solution of the equations of motion $\dot{\mathbf{\Gamma}}=\mathbf{F}(\mathbf{\Gamma})$. In particular, for the components associated with particle i we find

$$\dot{x}_i=p_i/m,$$

$$\dot{p}_i=(\lambda/N\sigma)\sum_{j\neq i}[2\Theta(x_j-x_i)-1],$$

where $\Theta(x)$ is the Heaviside step function. The flow is characterized by constant-force streaming, interrupted by discontinuous force jumps, when two particles cross. For each Lyapunov exponent we must consider, in addition to the reference trajectory $\mathbf{\Gamma}(t)$, a tangent vector $\delta\mathbf{\Gamma}(t)=\{\delta x_1,\ldots,\delta x_N,\delta p_1,\ldots,\delta p_N\}$ defined by

$$\delta\mathbf{\Gamma}(t)=\lim_{s\rightarrow 0}\frac{\mathbf{\Gamma}_s(t)-\mathbf{\Gamma}(t)}{s}, \quad (16)$$

where $\mathbf{\Gamma}_s(t)$ is an (infinitesimally) perturbed trajectory connected to $\mathbf{\Gamma}(t)$ by a parametrized path with parameter s such that $\lim_{s\rightarrow 0}\mathbf{\Gamma}_s(t)=\mathbf{\Gamma}(t)$. The time evolution of $\delta\mathbf{\Gamma}(t)$ is given by the linearized equations of motion, which for the components associated with i become

$$\delta\dot{x}_i=\delta p_i/m,$$

$$\delta\dot{p}_i=(2\lambda/N\sigma)\sum_{j\neq i}(\delta x_j-\delta x_i)\,\delta(x_j-x_i). \quad (17)$$

Between crossing events all δ functions are zero. Assuming that the last crossing of any particles occurred at time $t=0$, the tangent-vector components evolve according to

$$\delta x_i(t)=t\,\delta p_i(0)/m+\delta x_i(0),$$

$$\delta p_i(t)=\delta p_i(0). \quad (18)$$

If at some later time $t=t_{\rm coll}>0$ two particles, k and l, intersect, only the δ functions connecting these two particles contribute to Eq. (17), which for k becomes

$$\delta\dot{x}_k=\delta p_k/m,$$

$$\delta\dot{p}_k=(2\lambda/N\sigma)(\delta x_l-\delta x_k)\,\delta(x_l-x_k).$$

An integration from an instant immediately before $(-)$ to immediately after $(+)$ the crossing yields the instantaneous crossing map [21] for the tangent-vector components associated with particle k,

$$\delta x_k{}^{+}=\delta x_k{}^{-},$$

$$\delta p_k{}^{+}=\delta p_k{}^{-}+\frac{2\lambda}{N\sigma}\int_{t_c^-}^{t_{\rm coll}^+}(\delta x_l-\delta x_k)\,\delta(x_l-x_k)\,dt$$

$$=\delta p_k{}^{-}+\frac{2\lambda(\delta x_l-\delta x_k)_{t=t_{\rm coll}}}{N\sigma|(\dot{x}_l-\dot{x}_k)_{t=t_{\rm coll}}|}, \quad (19)$$

and similarly for l. The components associated with all other particles are unaffected by the crossing of k and l. Equations (18) and (19) suffice to construct the exact time evolution of a tangent vector $\delta\mathbf{\Gamma}(t)$ in tangent space.

The Lyapunov exponents are defined by

$$\lambda(\delta\mathbf{\Gamma}(0))=\lim_{t\rightarrow\infty}\frac{1}{t}\ln\frac{|\delta\mathbf{\Gamma}(t)|}{|\delta\mathbf{\Gamma}(0)|}.$$

According to Oseledec [32] there are L orthonormal initial vectors $\delta\mathbf{\Gamma}_l(0)$ yielding a set of exponents $\{\lambda_l\}, l=1,\ldots,L$, referred to as the Lyapunov spectrum. L is equal to the phase-space dimension $2N$ for our linear system. We order the exponents according to $\lambda_1\geqslant\lambda_2\geqslant\cdots\geqslant\lambda_L$. In the actual computation we follow the reference trajectory in phase space and, simultaneously, the complete set of tangent vectors in tangent space, from one interparticle crossing event to the next. The tangent vectors are periodically reorthonormalized, and the Lyapunov exponents are obtained from the time-averaged logarithms of the renormalizing factors [28–30].

Since for Hamiltonian systems the phase volume is conserved, any expansion in certain phase-space directions must be exactly compensated by a contraction in some other directions, and the sum of all Lyapunov exponents vanishes. Furthermore, due to the symplectic nature of the equations of motion, the Lyapunov exponents appear in conjugate pairs of equal magnitude and opposite sign. It suffices to determine only the positive exponents to obtain the full spectrum, a significant saving of computer time. For each quantity conserved by the phase flow one exponent vanishes. In the one-dimensional case the conservation of energy, of linear momentum, of the center of mass, and the neutral expansion behavior in the flow direction cause four of the exponents to vanish.

IV. COMPUTER SIMULATION

To test our theoretical expressions we have carried out extensive computer simulations for one-dimensional systems ($d=1$) defined by Eq. (1). In our numerical work we measure distances in units $L_0=\sigma$, mass in units of the particle mass, $M_0=m$, energies in units $E_0=\lambda$, and time in units $T_0=\sqrt{m\sigma^2/\lambda}$. In all our simulations the total energy per particle is taken to be unity in our reduced units, $E/(N\lambda)\equiv\epsilon/\lambda=1$. In the terminology of the linear sheet model (3) this means that the total mass $Ns=m$, the total energy ϵ, and $2\pi G$ are all unity, and that our dimensionless units for length, velocity, and time are given by

$$L_0=\frac{\epsilon}{2\pi G m^2},$$

$$V_0=\left(\frac{\epsilon}{m}\right)^{1/2},$$

$$T_0=\frac{1}{2\pi G m}\left(\frac{\epsilon}{m}\right)^{1/2}.$$

These units differ slightly from the various units used by other authors [21,22,16,9].

For the initial distribution we take a uniform distribution in the single-particle μ space, limited by the box $[x_{\min},x_{\max}]\times[p_{\min},p_{\max}]$. We characterize this initial condition by the ratio of the initial energy ratio $K(0)/E$ or, alternatively, by the virial ratio

$$\mathcal{V}(0)\equiv\frac{2K(0)}{\nu V(0)}=\frac{2}{\nu}\frac{[K(0)/E]}{1-[K(0)/E]},\tag{20}$$

the ratio of twice the kinetic energy to the product of ν and the potential energy, at time $t=0$. In microcanonical equilibrium $\mathcal{V}(t\to\infty)$ must approach 1, a necessary but not sufficient condition for equilibrium.

In the continuum limit such rectangular initial box configurations are usually referred to as ''waterbags'' [5,15], since in this limit the evolution of the collisionless Boltzmann (or Vlasov) equation is volume preserving in μ space [26] and results only in a deformation of the contour and not of the volume of the bag. The Vlasov equation has uncountably many stationary solutions [33] for the distribution function in μ space. One distinguished solution is the microcanonical distribution $f(p_1,x_1)=n(x_1)\rho(p_1)$, where for the sheet model the momentum- and particle-density distributions are explicitely given by Eqs. (12) and (14), respectively.

For the sheet model with a finite number of particles it is found [15] that any initial condition, sampled from such a rectangular box distribution, quickly relaxes towards a quasistationary distribution, which depends on its initial virial ratio, and which may differ significantly from the ultimate equilibrium distribution predicted by the microcanonical theory in Sec. II B. It is believed that these extremely long-lived quasistationary states converge, for $N\to\infty$, to the true stationary waterbag solutions of the Vlasov equation. The relaxation from this stage to the final microcanonical equilibrium is different for various ν and will be discussed below.

A. The sheet model, $\nu=1$

For all simulations with the sheet model we use an ''exact'' algorithm similar to that in Refs. [6,11], stepping from one crossing event of any two particles to the next. With double-precision arithmetic the total-energy conservation is of the order of 1 part in 10^{12} over the whole length of the runs, which stretch over 2×10^8T_0 and involve much more than 1×10^9 collisions. The length of these simulation runs is comparable only to those of most recent work [9] and is one order of magnitude larger than in previous studies [15].

A characteristic period t_c of oscillation for a typical particle may be estimated [34,35,16] according to $t_c=(\pi/Gmn_0)^{1/2}$, where $n_0=\beta\lambda/(4\sigma)$ is the equilibrium particle density at the origin. Since $\beta\simeq(3/2)(N/E)$ from Eq. (8), we find

$$t_c=2\pi\left(\frac{4}{3}\right)^{1/2}\frac{\sigma}{\lambda}\left(\frac{mE}{N}\right)^{1/2},$$

which is 7.3 in our reduced time unit. This may serve to estimate the number of particle oscillations during a given time.

We have mentioned already in the Introduction that the relaxation processes towards microcanonical equilibrium proceed (if at all) with much longer time scales [12,13] than originally suggested [10,11]. In a recent series of papers Tsuchiya, Konishi, and Gouda [15,16] used the initial rectangular box distributions as initial conditions for their simulations which involved between 64 and 1000 sheets. They concluded that three different time regimes may be distinguished. In the *first* regime, $0<t<T_m$, referred to as the collisionless phase, the initial arbitrary distribution of particle energies is only slowly relaxed with a so-called *microscopic relaxation* time $T_m\approx NT_0$. In the *second* regime, $T_m<t<T_M$, the system stays in a long-lived quasistationary state, the finite-particle analog of the stationary waterbag solution in the mean-field limit. The individual particle energies fluctuate diffusively such that the total energy is equally divided among all particles over an indefinitely long time. Finally, the so-called *macroscopic relaxation time* $T_M\approx4\times10^4NT_0$ (for $N\leqslant104$) marks the transition to the *third* regime, which is identified with microcanonical equilibrium. However, Yawn and Miller have noted most recently [9] that

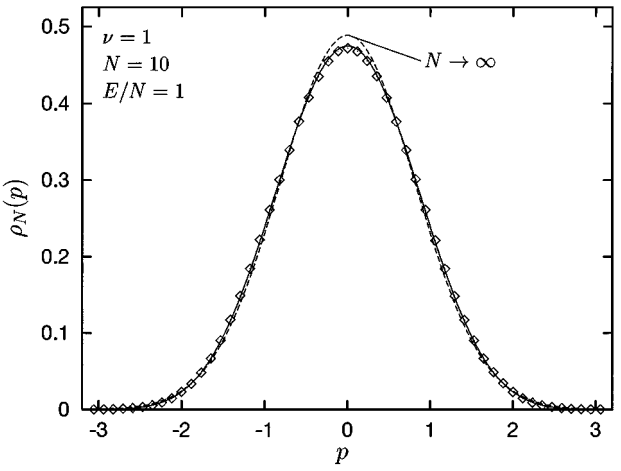

FIG. 1. Momentum distribution $\rho_{10}(p)$ for the sheet model ($d = \nu = 1$), with $N = 10$ sheets and initial conditions characterized by a virial ratio $\mathcal{V}(0) = 2$. The diamonds are simulation results, where the system evolved freely for $t_0 = 10^8 T_0$ prior to measuring the distribution. The smooth curve is the microcanonical equilibrium distribution according to Eq. (11), and the dashed curve is the Boltzmann distribution applicable in the thermodynamic limit, Eq. (12). The energy E is given in units of λ, and p and ρ_N are measured in units of mV_0 and $(mV_0)^{-1}$, respectively.

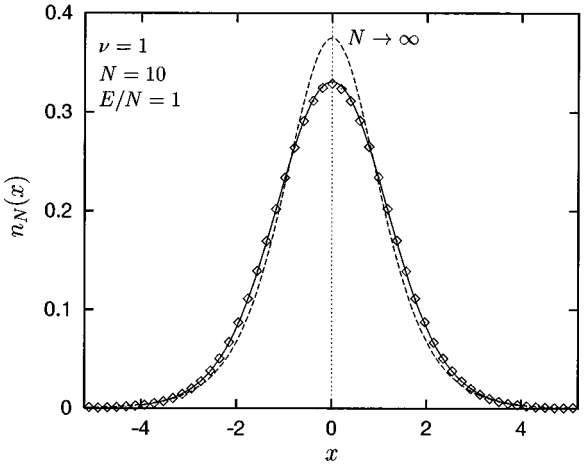

FIG. 2. Spatial particle distribution function $n_{10}(x)$ for the sheet model ($d = \nu = 1$), with $N = 10$ sheets and initial conditions characterized by a virial ratio $\mathcal{V}(0) = 2$. The diamonds are simulation results, where the system evolved freely for $t_0 = 10^8 T_0$ prior to measuring the distribution. The smooth curve is the equilibrium particle distribution according to Eq. (15), and the dashed curve is the mean-field approximation Eq. (14) applicable for large N. The energy E is given in units of λ, and x and n_N are measured in units of σ and σ^{-1}, respectively.

the equipartition of the energy among all particles is only a necessary and not a sufficient condition for equilibrium and that still doubts about the ergodicity of systems with $N > 10$ persist.

We have computed the momentum and particle distributions of medium-sized systems for which $10 \leqslant N \leqslant 64$. The averaging interval covers t_0 to $t_0 + 10^8 T_0$ with an offset time $t_0 \geqslant 7 \times 10^7 T_0$. According to the previous analysis we may safely expect, after t_0, that our systems are in microcanonical equilibrium, if they are ergodic. The least populated system we have studied contains 10 sheets. This corresponds to the critical population and, hence, to the largest N for which the phase space has been shown to be segmented into isolated regions with distinct ergodic properties [7]. In Figs. 1 and 2 we show, by the diamonds, the time-averaged momentum distribution $\rho_{10}(p)$ and the particle distribution $n_{10}(x)$, respectively, for this system. We compare these results to the respective predictions for microcanonical equilibrium from Eqs. (11) and (15) with $N = 10$, represented by the full lines. The agreement is very good. Only very small systematic differences between the simulation results and the microcanonical predictions may be detected, a consequence of the (statistically insignificant) regular domain in phase space supporting stable periodic orbits. Analogous conclusions have been reached already by Wright and Miller [13] for an even smaller system with $N = 6$. Also shown in Figs. 1 and 2, by the dashed curves, are the many-particle limits from Eqs. (12) and (14), respectively, where $\lim_{N \to \infty} kT = 2/3$ from Eq. (8) has been used. The comparison with the simulation data reveals that a 10-sheet system is not populous enough to be treated by mean-field theory [22].

As an example for larger N we display in Figs. 3 and 4 analogous data for a 40-sheet system. As expected, the comparison of the simulation results (diamonds) with the microcanonical predictions (smooth lines) is excellent, both for the momentum distribution $\rho_{40}(p)$ in Fig. 3 and the particle distribution $n_{40}(x)$ in Fig. 4. The system seems to be ergodic and capable of reaching microcanonical equilibrium. A comparison with the respective mean-field results (dashed curves) also suggests the usefulness of this limit for such small particle numbers.

The partition of the total energy into kinetic and potential contributions has also been tested. In all cases the virial relation (9) is well obeyed as may be verified from Table II.

For all 6 systems with $16 \leqslant N \leqslant 64$ investigated by us we

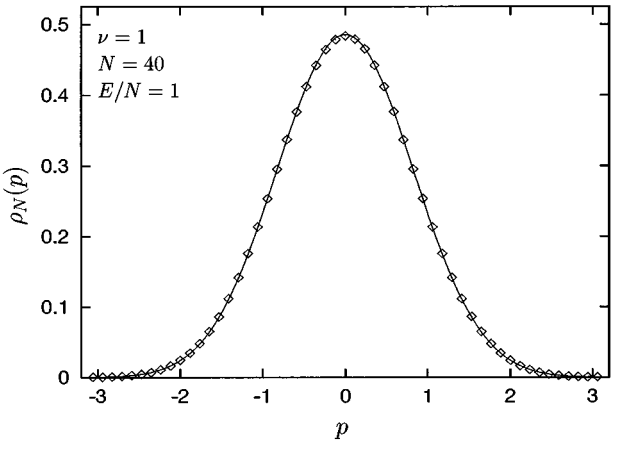

FIG. 3. Momentum distribution $\rho_{40}(p)$ for the sheet model ($d = \nu = 1$), with $N = 40$ sheets and initial conditions characterized by a virial ratio $\mathcal{V}(0) = 2$. The diamonds are simulation results, where the system evolved freely for $t_0 = 7 \times 10^7 T_0$ prior to measuring the distribution. The smooth curve is the microcanonical equilibrium distribution according to Eq. (11). The energy E is given in units of λ, and p and ρ_N are measured in units of mV_0 and $(mV_0)^{-1}$, respectively.

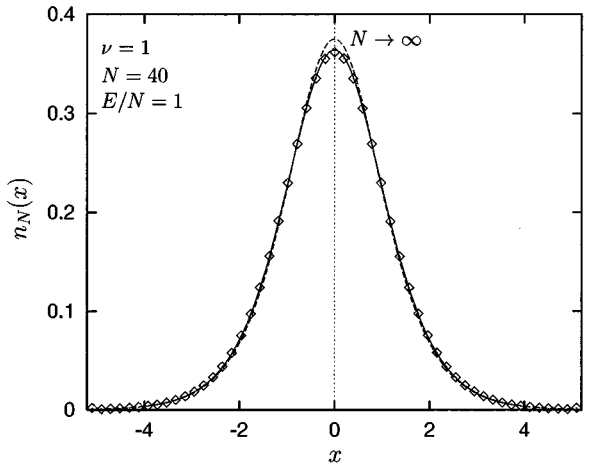

FIG. 4. Spatial particle distribution function $n_{40}(x)$ for the linear sheet model with 40 sheets. The diamonds are simulation results for initial conditions characterized by a virial ratio $K(0)/E = 0.5$. Prior to measuring the distribution the system evolved freely for 7×10^7 time units. The smooth curve is the equilibrium particle distribution according to Eq. (15), and the dashed curve is the mean-field approximation Eq. (14) applicable for large N. The energy E is given in units of λ, and x and n_N are measured in units of σ and σ^{-1}, respectively.

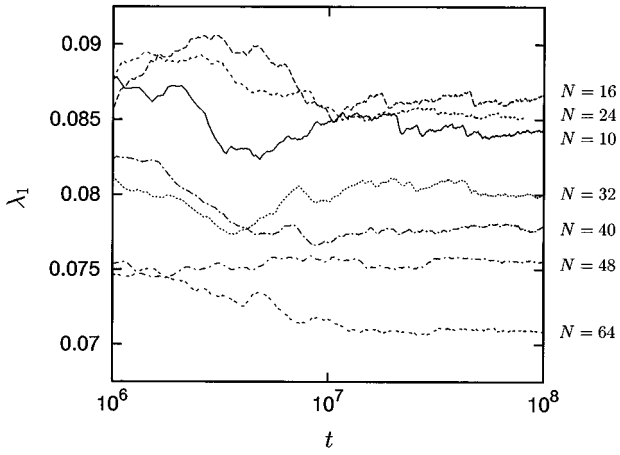

FIG. 5. Convergence of the maximum Lyapunov exponents $\lambda_1(t)$, as a function of the length of the averaging interval for sheet model ($d = \nu = 1$). The number of particles, N, is indicated by the labels. Prior to $t = 0$, at which time the time averaging for the Lyapunov exponents starts, the system is evolved for at least $7 \times 10^7 T_0$. Times are measured in units of T_0, and Lyaponov exponents in units of T_0^{-1}.

find similar good agreement for the computed distributions with their corresponding microcanonical equilibrium analogs as displayed for $N = 40$ in Figs. 3 and 4. However, the very good agreement for $N = 10$ in Figs. 1 and 2 and for $N = 6$ in Ref. [13], systems for which it is known that the microcanonical equilibrium does not exist [7], conveys the warning that this comparison is not a sensitive test for ergodicity. The extremely slow convergence of the distributions to their microcanonical predictions suggest that small stable and hitherto undetected regions associated with stable periodic orbits may persist in the phase space even for $N > 10$ [9].

As another probe for the study of the thermalization properties the computation of the Lyapunov exponents has been suggested [21,7,15]. We report here the full Lyapunov spectra for systems containing $N = 10$, 16, and 24 particles. For the larger systems studied here, with particle numbers ranging from 32 to 64, only the two largest exponents λ_1 and λ_2 were computed. The convergence of the respective maximum exponents λ_1 is shown in Fig. 5, where the time was reset to $t = 0$ after the end of the thermalization period t_0, which lasted for at least 7×10^7 time units (10^6 periods of oscillation). These curves reveal an interesting behavior for $t > 10^7$ and the smaller values of N: the Lyapunov exponents, cumulatively averaged from time t_0 (for which the systems are believed to be already in microcanoncial equilibrium) to $t_0 + t$, show a tendency to increase slowly with t until they drop in a random and intermittent fashion to a slightly smaller value within a comparatively short time. This indicates that the phase trajectory is intermittently ''caught'' in a rather restricted region of the phase space with much less violent expansion properties in tangent space. This causes the cumulative average of the exponents to drop sharply. Such regions have been referred to as ''stagnant layers'' [15] or ''sticky regions'' [9] and are known to occur near the boundary of regularity islands in phase space. Only after the trajectory escapes from such a region may the value of the exponents go up again.

In Fig. 6 the Lyapunov spectra for 10-, 16-, and 24-particle systems are shown. All spectra are normalized by their respective maximum exponents λ_1, and on the abscissa we use $(N-l)/(N-1)$. The index l enumerates conjugate pairs of exponents such that the most positive and negative exponents, λ_1 and λ_{2N}, are associated with $l = 1$, the second-largest exponent λ_2 and second-smallest exponent λ_{2N-1} with $l = 2$, and, finally, the four vanishing exponents $\lambda_{N-1}, \ldots, \lambda_{N+2}$ with the indexes $N-1$ and N. For each spectrum only the positive branch is shown, which includes N exponents $\geqslant 0$ indicated by the points. Since the spectra are for equilibrium systems, the conjugate negative branch

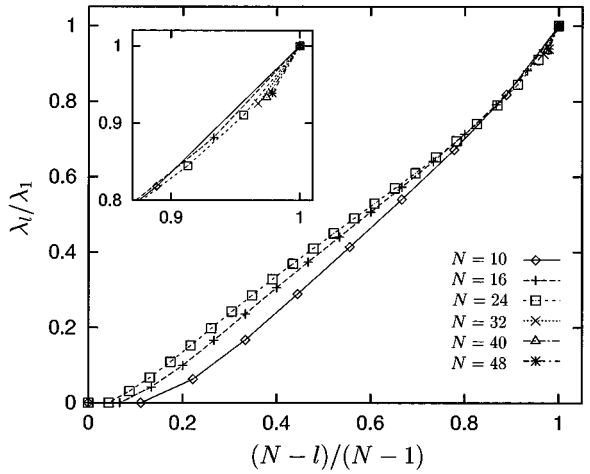

FIG. 6. Reduced Lyapunov spectra for $N = 10$, 16, and 24 particles, as indicated by the labels, for the sheet model ($d = \nu = 1$). In the inset a magnified view of the largest exponents is shown, which includes also results for systems with $N = 32$, 40, and 48. The Lyaponov exponents are given in units of T_0^{-1}.

TABLE I. Selected Lyapunov exponents and the Kolmogorov-Sinai entropy per particle are listed for the sheet model, $\nu=1$, $d=1$, and $E/N\lambda=1$, in equilibrium. N is the particle number, λ_1, λ_2, and λ_{N-2} are the maximum, the second largest, and the smallest positive Lyapunov exponents, respectively, and h_{KS}/N is the Kolmogorov-Sinai entropy per particle. The error for the exponents is estimated from convergence plots similar to Fig. 5 and is about $\pm 0.5\%$ for λ_1,λ_2, and $\pm 1.5\%$ for λ_{N-2}. All exponents and h_{KS} are listed in units of T_0^{-1}.

N	λ_1	λ_2	λ_{N-2}	h_{KS}/N
10	0.0842	0.0689	0.00535	0.0334
16	0.0864	0.0762	0.00363	0.0366
24	0.0854	0.0777	0.00265	0.0375
32	0.0804	0.0745		
40	0.0778	0.0726		
48	0.0757	0.0710		
64	0.0711			

may be obtained as the mirror image around the abscissa. Only the points have physical significance; the lines are only drawn for clarity. In the inset we display the largest exponents for all spectra and include also data for $32\leqslant N\leqslant 64$. As noted already in Sec. III, four exponents vanish for each spectrum, of which two are shown in Fig. 6. The two largest exponents, λ_1,λ_2, and, where available, the smallest positive exponent λ_{N-2}, and the Kolmogorov-Sinai entropy per particle, h_{KS}/N, are listed in Table I for various N.

In Fig. 7 we compare our equilibrium values for the maximum Lyapunov exponent λ_1 (full squares) with the results taken from Fig. 13 of Tsuchiya, Konishi, and Gouda [15]. The agreement in the range of overlapping N is very good. The maximum for $N\approx 16$ indicates the system population with the strongest phase-space expansion for (infinitesimal) perturbations. In the same figure we also compare our results

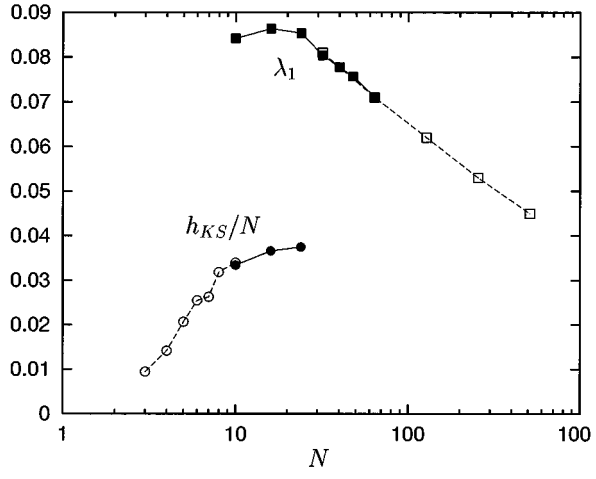

FIG. 7. Particle-number dependence of the maximum Lyapunov exponent λ_1 (squares) and of the Kolmogorov-Sinai entropy per particle, h_{KS}/N, for the sheet model. These quantities are given in units of T_0^{-1} introduced in the text. The full squares and dots are results of this work. The exponents represented by open squares are from Tsuchiya *et al.* [15], and the data for h_{KS}/N represented by circles are from Benettin *et al.* [21].

TABLE II. Tabulation of the virial ratio $\overline{\mathcal{V}}$, averaged over a time interval in the equilibrium (or quasistationary) states at the end of the runs, for the one-dimensional models with potential parameter ν. The initial conditions are characterized by the initial virial ratio $\mathcal{V}(0)$, and N is the number of particles. Times are given in units of T_0.

ν	N	$\mathcal{V}(0)$	$\overline{\mathcal{V}}$
1.0	16	2.00	1.0008
1.0	40	2.00	0.9995
1.5	16	1.33	1.0029
1.5	40	0.15	1.0018
1.5	40	0.57	1.0018
1.5	40	1.33	1.0038
1.5	40	3.11	1.0050
1.5	40	12.00	0.9997
4.5	40	0.44	1.0000

for the Kolmogorov-Sinai entropy per particle, h_{KS}/N (full dots), with the data reported by Benettin, Fröschle, and Scheidecker [21] for $3<N<10$. These authors conjectured that h_{KS} increases linearly with N already for $N>2$. Our extended plot reveals, however, that such a linear dependence is reached, if at all, only for N exceeding 24. There seems to exist a crossover population $N_c\approx 12$ where the N dependence of h_{KS} changes qualitatively. It is likely that this number is related to the critical population of Reidl and Miller [7] for the (proven) existence of regions in phase space supporting stable periodic orbits.

B. The case $\nu=1.5$

For $\nu\neq 1$ the force between the particles depends on their separation and no analytical solution for the particle trajectories between successive encounters of any two particles can be given. In our exploratory work for $\nu=1.5$ we have therefore resorted to a resource-saving, but cruder, approach by solving the equations of motion with a Gear predictor-corrector algorithm [36], accurate to $O(\Delta t^5)$ in the time step, and with a fixed time step $\Delta t=0.002$. In spite of this gross simplification the resulting code is still 20 times less efficient than the program for $\nu=1$. This algorithm is not symplectic, but the relative energy fluctuations do not exceed 0.06% for the full length of the respective runs. This was considered sufficient for our survey.

Starting with an initial box distribution as before, the system very quickly relaxes into a quasistationary state that depends strongly on the initial virial ratio $\mathcal{V}(0)$. The virial ratio $\overline{\mathcal{V}}$, time averaged over an interval in this regime and listed in Table II, is very close to unity. The system virializes, but the momentum and particle density distributions differ significantly from the microcanonical equilibrium distributions, as is demonstrated in Fig. 8 for $0.148\leqslant\mathcal{V}(0)\leqslant 12$. Such behavior is reminiscent of the sheet model in Sec. IV A, but here the states are so stable that even after our longest simulation runs no macroscopic relaxation towards microcanonical equilibrium could be detected. For 16 and 40 particles we followed the trajectory for 7×10^6 and 6×10^6 time units T_0,

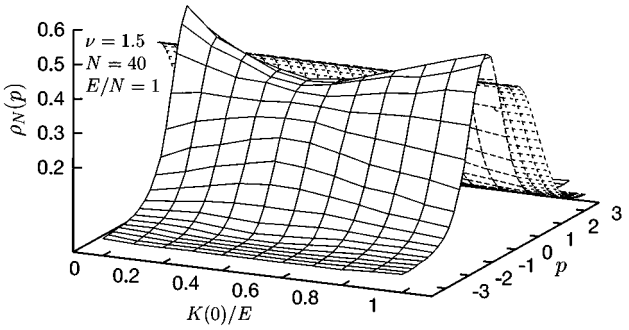

FIG. 8. Momentum distributions $\rho_{40}(p)$ for the linear system with $\nu=1.5$ and $N=40$ particles. The initial conditions are characterized by the energy ratio $K(0)/E$. For positive momenta p also the microcanonical equilibrium distribution is shown by the dotted surface. The distributions are time averages in the interval $1.1T_0 \times 10^5 < t < 2.1 \times 10^5 T_0$. The energy E is measured in units of λ, p in units of mV_0, and ρ_N in units of $(mV_0)^{-1}$.

much longer than the average macroscopic relaxation time T_M found for the sheet models of comparable size [16]. We demonstrate this stability of the quasistationary equilibrium states in Fig. 9 for $K(0)/E=0.5$ corresponding to $\mathcal{V}(0)=4/3$, the broadest of the momentum distributions depicted in Fig. 8. The smooth line in Fig. 9 refers to microcanonical equilibrium Eq. (11), whereas the symbols indicate simulation results for $\rho_{40}(p)$ for different averaging time intervals: $0<t<10^6 T_0$ (diamonds), $10^6 T_0<t<2\times10^6 T_0$ (crosses), and $2\times10^6 T_0<t<3\times10^6 T_0$ (squares). Corresponding results for the spatial particle distributions $n_N(x)$ are shown in Fig. 10, where the symbols have the same meaning as before, and where the dashed curve is the mean-field solution of Eq.

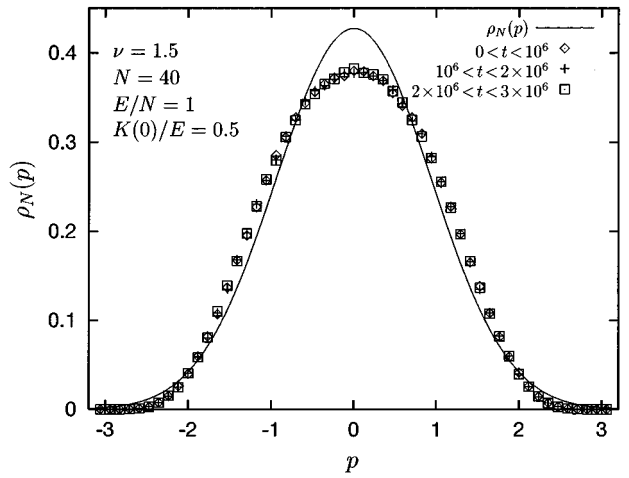

FIG. 9. Momentum distribution $\rho_{40}(p)$ for the one-dimensional model with $\nu=1.5$, and $N=40$. The initial virial ratio $\mathcal{V}(0)=4/3$ corresponds to $K(0)/E=0.5$. The various symbols are simulation results and, as indicated by the labels, refer to the time interval used for averaging. The smooth curve is the analytical equilibrium distribution according to Eq. (11). The energy E and times are given in units of λ and T_0, respectively, p is measured in units of mV_0, and ρ_N in units of $(mV_0)^{-1}$.

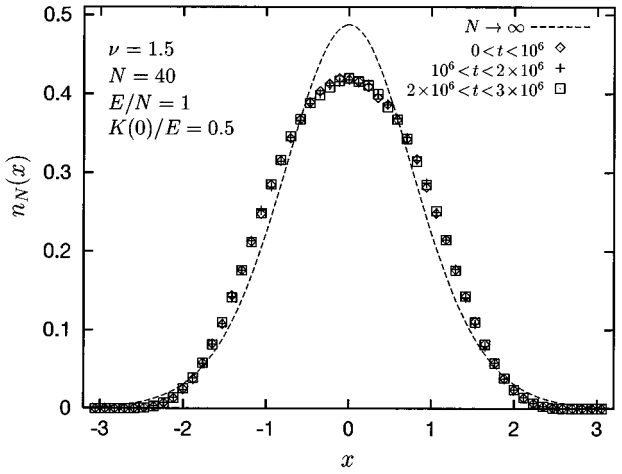

FIG. 10. Spatial particle distribution $n_{40}(x)$ for the one-dimensional model $\nu=1.5$, and $N=40$. The virial ratio $\mathcal{V}(0)=4/3$ corresponds to $K(0)/E=0.5$. The various symbols are simulation results and, as indicated by the labels, refer to the time interval used for averaging. The dashed curve is the mean-field solution of Eq. (13) obtained numerically by iteration. The energy E is given in units of λ, time in units of T_0, distance in units of σ, and n_N in units of σ^{-1}.

(13). For consistency the latter was computed with a temperature obtained by taking the $N\to\infty$ limit of Eq. (8): $kT=6/7$. The mean-field particle density is expected to be already a good representation for the exact equilibrium density distribution for $N=40$.

C. The case $\nu=4.5$

This result, the lack of an observable macroscopic relaxation of the various distribution functions towards equilibrium for $\nu=1.5$, led us to examine also a one-dimensional system with a value of ν far from the regular harmonic-oscillator case $\nu=2$, namely, $\nu=4.5$. The same algorithm as

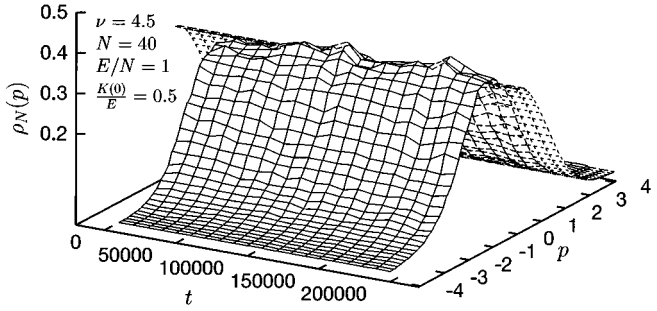

FIG. 11. Relaxation of the momentum distribution $\rho_N(p)$ towards its equilibrium distribution for the linear model with $\nu=4.5$, and $N=40$. The virial ratio $\mathcal{V}(0)=4/3$ corresponds to $K(0)/E=0.5$. The distributions are shown for various run times t. Each distribution is an average over a time interval of width $10^4 T_0$. Also displayed, for positive p, is the equilibrium distribution computed from Eq. (11). The total energy E and the time are given in units of λ and T_0, respectively, p is measured in units of mV_0, and ρ_N in units of $(mV_0)^{-1}$.

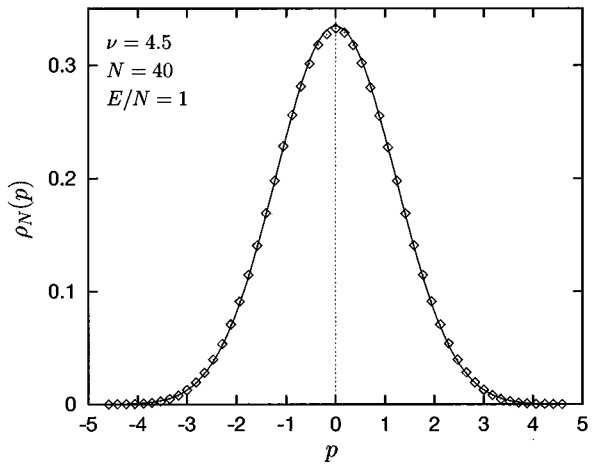

FIG. 12. Momentum distribution $\rho_{40}(p)$ for the linear model with $\nu=4.5$, and $N=40$. The initial virial ratio $\mathcal{V}(0)=0.444$ The symbols are simulation results, averaged in the interval $2\times10^5T_0 < t < 2.2\times10^6T_0$. The smooth curve is the microcanonical equilibrium distribution Eq. (11). The energy E is given in units of λ, p in units of mV_0, and ρ_N in units of $(mV_0)^{-1}$.

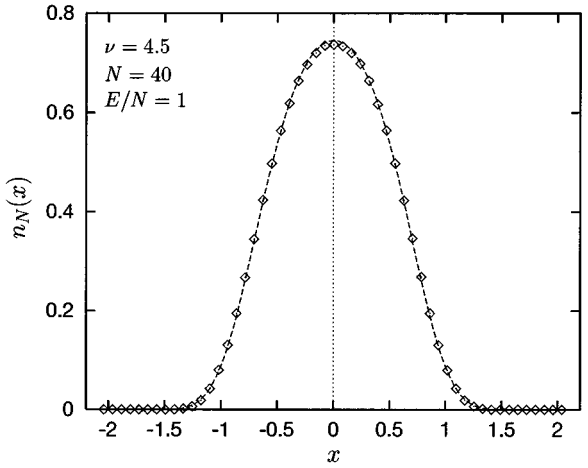

FIG. 13. Spatial particle distribution $n_{40}(x)$ for the one-dimensional model with $\nu=4.5$, and $N=40$. The initial virial ratio $\mathcal{V}(0)=0.444$ The symbols are simulation results, sampled and averaged in the interval $2\times10^5T_0<t<2.2\times10^6T_0$. The smooth curve is the mean-field solution of Eq. (13) obtained numerically by iteration. The energy E is given in units of λ, x in units of σ, and n_N in units of σ^{-1}.

in Sec. IV B was used. But the results are quite different and much more in accord with physical intuition, as becomes obvious from Fig. 11. There the ''instantaneous'' momentum distribution $\rho_{N=40}(p)$ for a 40-particle system is shown at various times t during the run, starting from an initial condition with $\mathcal{V}(0)=0.444$. As in all our simulations $E/N=1$ in our reduced units. We observe that after a time of 2×10^5T_0 the system reaches thermal equilibrium and remains in it thereafter. The nonlinearity of the force introduced by $\nu=4.5$ suffices to enhance mixing in phase space, and the final distributions are independent of the initial conditions.

The momentum and spatial particle distributions for this equilibrated model are shown in Figs. 12 and 13, respectively, where the averaging interval was $2\times10^5T_0<t<2.2\times10^6T_0$. The experimental distributions (diamonds) are compared to the respective theoretical predictions shown as dashed curves, the exact momentum distribution Eq. (11) in Fig. 12, and the mean-field approximation Eq. (13) in Fig. 13. The latter was obtained by numerical iteration of Eq. (13) with an initial Gaussian trial function. To be consistent, the microcanonical temperature for finite N, Eq. (8), was not used for this calculation, but instead $\lim_{N\to\infty}kT=18/13\lambda$. For $N=40$ the mean-field solution $n(x)$ is expected to deviate only very little from the hitherto unknown exact result for $\nu=4.5$. The agreement between simulation and theory is very good in all cases. Also the partition of the total energy into potential and kinetic contributions, Eq. (9), is well obeyed by the simulation results, as may be verified from $\overline{\mathcal{V}}$ listed in Table II.

V. DISCUSSION

In this paper we study the microcanonical equilibrium states of many-body systems (1) interacting with a power-law potential and positive power ν. We derived the relation between temperature and energy for arbitrary dimension d and arbitrary ν. For the special case of one-dimensional systems we obtained also the microcanonical momentum distribution function in μ space. These results are generalizations to arbitrary d and/or ν of well-known results for $d=\nu=1$, the so-called sheet model [22]. We compared these theoretical results to extensive computer simulations and found excellent agreement for the sheet model. This confirms earlier results by Wright and Miller [13]. Also another one-dimensional system, $\nu=4.5$, provided excellent agreement between simulation and microcanonical prediction. However, no agreement was found for an intermediate case, namely, $\nu=1.5$. This system stubbornly refused to relax to microcanonical equilibrium and remained in a quasistationary state over the whole length of the runs, which were of considerable length. The momentum and density distribution functions of these quasistationary states depend on the selected nonequilibrium initial condition.

For the sheet model we applied an exact algorithm, first developed by Benettin [21], to the computation of the complete Lyapunov spectrum for less populated systems for which $N\leqslant24$. Since the algorithm for the dynamics derived from Eq. (3) is not parallelizable in principle, the question of extending our simulations to larger N is closely linked to the available hardware. We were able to compute the maximum Lyapunov exponent for $N\leqslant64$ and are working to extend this range to larger N [31]. Although at present the limited range of N for the available data (see Table I) does not allow the construction of the large-particle limit for the reduced Lyapunov spectra depicted in Fig. 6, our results make it very likely that such a limit exists, as is suggested by theory [37]. We also found in Fig. 7 that the Kolmogorov-Sinai entropy seems to increase linearly with the number of sheets for $N>24$. A similar statement has been given before [21], but this claim was based on data restricted to the range $3\leqslant N \leqslant10$, for which this proportionality does not apply. The

crossover population $N_c \approx 12$ is only slightly larger than the critical population of Reidl and Miller [7]. But further data for larger N are required before any conclusions can be reached. To our knowledge no theoretical predictions exist for the mean-field limit of h_{KS}/N.

A key issue for many-body systems is the mixing in phase space and the relaxation from an arbitrary initial condition to equilibrium. For the sheet model ($d=\nu=1$) it is well known that, at least for $N \leqslant 10$, the phase space is separated into confined and unconnected regions, one chaotic and at least one regular, which supports stable periodic orbits and KAM tori [7]. Also for $N>10$ doubts about ergodicity still persist [9]. We find here for $N \geqslant 10$ that after a few million characteristic periods of oscillations t_c the systems have relaxed to a state, presumably the equilibrium state for $N>10$, with a well-defined maximum Lyapunov exponent and, where available, a well-defined positive Kolmogorov-Sinai entropy per particle h_{KS}/N. These numbers are listed in Table I. $1/h_{\mathrm{KS}}$ is the characteristic time it takes for the phase flow to distribute a large number of states, initially in a small ball, over the whole phase space [19,18]. It is surprising that this time is rather short, whereas relaxation to microcanonical equilibrium takes place on a much longer time scale. The convergence properties of the maximum exponent for $N \leqslant 32$ in Fig. 6 suggest that even in ''equilibrium,'' to which this figure applies, there exist regions in phase space that contribute little to the growth of small perturbations and in which an arbitrary phase trajectory spends considerable time in an intermittent fashion. This leads to rather well-defined drops of the maximum exponent during the averaging process from which it recovers only slowly by moving back into the chaotic sea. The intermittent behavior can only be observed properly if the time averaging for the Lyapunov exponents is initiated in the equilibrium phase. Whether these ''sticky'' [9] or ''stagnant'' [15] regions form the neighborhood of regularity islands is not clear.

The lack of any observable relaxation towards equilibrium for the one-dimensional systems with $\nu=1.5$ in Sec. IV B is surprising. The quasistationary distributions, generated within a few thousand oscillation periods from the initial box (waterbag) conditions in μ space, virialize and persist unchanged for simulation runs lasting for a few million time units. We do not believe that this result is influenced by the fact that these simulations were carried out with a simplified and nonsymplectic algorithm, since computational noise would lead to enhanced mixing in phase space. It seems that the global relaxation time T_M increases if ν is raised from its sheet-model value, unity, to 1.5. It diverges for ν approaching the critical value 2 for the harmonic oscillator potential. This view is supported by the results presented in Sec. IV C for systems with $\nu=4.5$. The nonlinearity of this pair potential is large enough to induce sufficient mixing in phase space. At present no Lyapunov exponents and Kolmogorov-Sinai entropies are available for $\nu \neq 1$. Such data are planned to be reported in our future work [31].

ACKNOWLEDGMENTS

We are grateful to Dr. Ch. Dellago, Professor J.R. Dorfman, Professor Y. Elskens, Professor Wm. G. Hoover, Professor B. N. Miller, and Professor H. van Beijeren for valuable comments. The critical remarks and suggestions by Y. Elsken and B. N. Miller were particularly helpful for the completion of the final version of the manuscript. The authors gratefully acknowledge financial support from the Fonds zur Förderung der wissenschaftlichen Forschung, Grant No. P11428-PHY, and the allocation of computer resources by the Computer Center of the University of Vienna.

[1] W. Braun and K. Hepp, Commun. Math. Phys. **56**, 101 (1977).
[2] J.H. Oort, Bull. Astron. Inst. Netherlands **6**, 289 (1932).
[3] G. L. Camm, Mon. Not. R. Astron. Soc. **110**, 305 (1950).
[4] O. C. Eldrige and M. Feix, Phys. Fluids **6**, 398 (1963).
[5] M. Luwel and G. Severne, Astron. Astrophys. **152**, 305 (1985).
[6] G. Severne and M. Luwel, Astrophys. Space Sci. **122**, 299 (1986).
[7] C. J. Reidl, Jr. and B. N. Miller, Phys. Rev. E **48**, 4250 (1993).
[8] K. R. Yawn, B. N. Miller, and W. Maier, Phys. Rev. E **52**, 3390 (1995).
[9] K. R. Yawn and B. N. Miller, Phys. Rev. E **56**, 2429 (1997).
[10] F. Hohl and D. T. Broaddus, Phys. Lett. **25A**, 713 (1967).
[11] F. Hohl and M. R. Feix, Astrophys. J. **167**, 1166 (1967).
[12] H. L. Wright, B. N. Miller, and W. E. Stein, Astrophys. Space Sci. **84**, 421 (1982).
[13] H. L. Wright and B. N. Miller, Phys. Rev. A **29**, 1411 (1984).
[14] C. J. Reidl, Jr. and B. N. Miller, Phys. Rev. A **46**, 837 (1992).
[15] T. Tsuchiya, T. Konishi, and N. Gouda, Phys. Rev. E **50**, 2607 (1994).
[16] T. Tsuchiya, N. Gouda, and T. Konishi, Phys. Rev. E **53**, 2210 (1996).
[17] K. R. Yawn and B. N. Miller, Phys. Rev. Lett. **79**, 3561 (1997).
[18] Ch. Dellago and H. A. Posch, Phys. Rev. E **55**, R9 (1997).
[19] N. S. Krylov, in *Works on the Foundation of Statistical Mechanics*, edited by A. S. Wightman and P. W. Anderson (Princeton University Press, Princeton, 1979); Ya. G. Sinai, *ibid.* p. 239.
[20] Ja. B. Pesin, Sov. Math, Dokl. **17**, 196 (1976).
[21] G. Benettin, C. Froeschle, and J. P. Scheidecker, Phys. Rev. A **19**, 2454 (1979).
[22] G. B. Rybicki, Astrophys. Space Sci. **14**, 56 (1971).
[23] M. Hénon, Astron. Astrophys. **114**, 211 (1983).
[24] P. Debye and E. Hückel, Phys. Z. **24**, 185 (1923).
[25] R. Balescu, *Statistical Mechanics of Charged Particles* (Interscience Publishers, London, 1963).
[26] J. Binney and S. Tremaine, *Galactic Dynamics* (Princeton University Press, Princeton, 1987).
[27] H. A. Posch, H. Narnhofer, and W. Thirring, Phys. Rev. A **42**, 1880 (1990).
[28] G. Benettin, L. Galgani, A. Giorgilli, and J.-M. Strelcyn, Meccanica **15**, 9 (1980).
[29] I. Shimada and T. Nagashima, Prog. Theor. Phys. **61**, 1605 (1979).
[30] A. Wolf, J. B. Swift, H. L. Swinney, and J. A. Vastano, Physica D **16**, 285 (1985).

[31] Lj. Milanović, H. A. Posch, and W. Thirring (unpublished).
[32] V. I. Oseledec, Trans. Moscow Math. Soc. **19**, 197 (1968).
[33] K. H. Prendergast, Astron. J. **59**, 260 (1954).
[34] M. Luwel, G. Severne, and P. J. Rousseeuw, Astrophys. Space Sci. **100**, 261 (1984).
[35] C. J. Reidl, Jr. and B. N. Miller, Astrophys. J. **332**, 619 (1988).
[36] C. W. Gear, *Numerical Initial Value Problems in Ordinary Differential Equations* (Prentice-Hall, Englewood Cliffs, 1971).
[37] Y. G. Sinai, Int. J. Bifurcation Chaos Appl. Sci. Eng. **6**, 1137 (1996).